Carbon Dioxide Adsorption on Iron (III) Oxide Pillarized Na-Montmorillonite
(Penjerapan Karbon Dioksida pada Ferum (III) Oksida Terpilar Na-Montmorilonit)

Muhammad Nauval Farras Russamsi[1], Firman Joshua Nainggolan[1], Triati Dewi Kencana Wungu[1,2,3,*] & Suprijadi[1,2,3]

[1]*Graduate Program of Nanotechnology, Institut Teknologi Bandung, Jalan Ganesha 10 Bandung, West Java, Indonesia*
[2]*Physics Department, Faculty of Mathematics and Natural Sciences, Institut Teknologi Bandung, Jalan Ganesha 10 Bandung, West Java, Indonesia*
[3]*Research Center for Nanosciences and Nanotechnology, Institut Teknologi Bandung, Jalan Ganesha 10 Bandung, West Java, Indonesia*

ABSTRACT

Iron (III) oxide (Fe_2O_3) pillarized Na-montmorillonite (NaMMT) was prepared by ion-exchanging and calcining three different concentrations (0.025, 0.05, and 0.075 M) of $Fe(OH)_3$ with NaMMT. The obtained materials were then examined for its ability to capture carbon dioxide, using thermogravimetric methods. The structural, compositional, and textural changes caused by pillarization were also examined using XRD, XRF, FTIR, and BET-BJH. The results showed that NaMMT-0.025 (pillared using 0.025 M of $Fe(OH)_3$) and NaMMT-0.075 exhibit superior adsorption capacity compared to NaMMT, with NaMMT-0.025 having the greatest capacity. By contrast, NaMMT-0.05 registers a decrease in the amount of CO_2 adsorbed, compared to NaMMT. Using XRF, it was shown that the amount of Fe_2O_3 present in the samples correspond to the concentration of $Fe(OH)_3$ used in ion-exchange. XRD results shows that the interlayer space of NaMMT barely changed after addition of Fe_2O_3. Using FTIR, successful pillarization of Fe_2O_3 is confirmed, and by combining it with BET-BJH, it shows that addition of Fe_2O_3 could enhance carbon capture by creating favourable pore structures. Overall, it shows that adding an appropriate amount of Fe_2O_3 to montmorillonite will enhance CO_2 adsorption.

Keywords: Adsorption; carbon dioxide; montmorillonite; pillarization

ABSTRAK

Ferum (III) oksida (Fe_2O_3) terpilar dalam Na-montmorilonit (NaMMT) telah disiapkan dengan cara menukar ion tiga kepekatan berbeza $Fe(OH)_3$ (0.025, 0.05, dan 0.075 M) dengan NaMMT, kemudian memanggangnya. Bahan yang diperoleh kemudian diperiksa untuk keupayaannya menangkap karbon dioksida menggunakan kaedah termogravimetri. Perubahan struktur dan komposisi akibat pilari pun juga telah diperiksa menggunakan XRD, XRF, FTIR dan BET-BJH. Hasil kajian menunjukkan bahawa NaMMT-0.025 (dipilar menggunakan 0.025 M $Fe(OH)_3$) dan NaMMT-0.075 menunjukkan kapasiti penyerapan yang lebih unggul berbanding dengan NaMMT, dengan NaMMT-0.025 menunjukkan kapasiti terbesar. Sebaliknya, NaMMT-0.05 menunjukkan penurunan jumlah CO_2 yang diserap berbanding dengan NaMMT. Menggunakan XRF, didapati jumlah Fe_2O_3 dalam sampel sepadan dengan kepekatan $Fe(OH)_3$ yang digunakan dalam pertukaran ion. Hasil XRD menunjukkan ruang antara lapisan pada NaMMT hanya berubah sedikit disebabkan oleh penambahan Fe_2O_3. Menggunakan FTIR, pemilaran Fe_2O_3 disahkan berjaya dan dengan menggabungkannya dengan hasil BET-BJH, didapati bahawa penambahan Fe_2O_3 dalam jumlah yang sesuai membina struktur liang yang menggalakkan penyerapan CO_2. Secara keseluruhannya, ini menunjukkan bahawa penambahan jumlah Fe_2O_3 yang sesuai ke dalam montmorilonit akan meningkatkan penyerapan CO_2.

Kata kunci: Karbon dioksida; montmorilonit; pemilaran; penyerapan

Introduction

Climate change caused by anthropogenic activities is one of the most consequential problems affecting humanity. One major cause of climate change is the ever-increasing amount of greenhouse gases, most commonly carbon dioxide, in the atmosphere. Since the industrial revolution began in the 18th century, the amount of CO_2 has steadily risen, from 280 ppm in 1750 to 360 ppm in the year 2000 (Eggleton 2012).

To mitigate climate change, the world must dramatically reduce carbon emissions. This is done by both switching to noncarbon forms of energy such as nuclear, wind, hydropower, and solar, and by utilizing carbon-capture and storage technologies. The Intergovernmental Panel on Climate Change has identified carbon capture and storage as an essential element in mitigating climate change (Rubin et al. 2005). Many carbon capture solutions have been developed, and carbon capture using solid adsorbents, because of its simplicity and cost-effectiveness, is considered the most viable way going forward (Raganati, Miccio & Ammendola 2021).

Clay is classified within the category of aluminophyllosilicate minerals. This categorization signifies that its primary structure is composed of alternating layers of silicon (Si) and aluminium (Al) atoms. Empty regions called interlayer space can be found between these layers, which can be filled with various atoms, ions, or molecules. Compared to other materials used for adsorbing CO_2, clays have the advantage of being extremely cost-effective and exhibiting good thermal stability. However, natural clays have a low adsorption capacity, which significantly impacts its viability for carbon capture (Raganati, Miccio & Ammendola 2021). Kaolin, for instance, has shown a CO_2 adsorption capacity of 0.106 mmol/g (Quiroz-Estrada et al. 2016) while montmorillonite (MMT) has a capacity of 0,114 mmol/g (Wang et al. 2020). The adsorption capacity for montmorillonite is slightly higher, which is attributed to its larger specific surface area due to the presence of micropores and a greater number of adsorption sites for CO_2 within the interlayer spaces of montmorillonite (Wang et al. 2020).

As such, clays must be modified to improve its adsorption characteristics. One simple, cost-effective, environmentally friendly, and cost-effective methods is pillarization. Pillarization is the process of introduction or doping of atoms, ions, and/or molecules into the interlayer spaces of clay. One of the most common elements used in pillarization is metal or metal oxides, which is usually done by exchanging between already-present charge-compensating cations and metal/metal hydroxide cations (Bineesh et al. 2010). Upon calcination, these cations are converted into pillars inside the interlayer space.

If done properly, pillarization by metal or metal oxides causes the interlayer space of the clay to be further apart and promotes the formation of micropores. These changes causes pillarized clays to have excellent adsorption and catalytic characteristics. Thus, metal or metal oxide pillared clays have been investigated for many purposes, most commonly as catalysts (Feng et al. 2018) and adsorbents for both water (Desai, Kannan & Reddy 2023) and soil pollution (Kumaraja et al. 2017).

Metal or metal-oxide pillared clays has also been investigated for carbon capture. Studies has shown an improvement in CO_2 adsorption capacity when montmorillonite was combined with elemental nanoscale iron, also called nano zero-valent iron (NZVI) (Bouazizi et al. 2017). Because NZVI tend to oxidize when exposed to air, the synthesis process and the storage of the resulting material need to occur in an inert atmosphere (Ruiz Torres et al. 2018). This requirement can be expensive and present practical challenges. In contrast, the use of iron oxides presents no such problem.

In this paper, iron (III) oxide (Fe_2O_3) with three different concentrations are used to pillarize sodium montmorillonite (Na-MMT). Fe_2O_3 pillared montmorillonite has been investigated for use as adsorbents for herbicides (Marco Brown et al. 2012) and radioactive materials (Hristodor et al. 2013), which crucially shows favourable characteristics for carbon capture such as bigger specific surface area and interlayer space. A series of Fe_2O_3 pillared clays with different concentrations of pillaring agent was synthetized. CO_2 adsorption capacity of the materials was investigated using thermogravimetric methods. To analyse the structural and compositional changes caused by Fe_2O_3 pillarization, XRD, XRF, FTIR, and BET-BJH analysis using N_2 adsorption isotherm was employed.

Materials and Methods

The materials used are NaMMT (MMT K10, Sigma-Aldrich), $FeCl_3$ (ROFA Laboratorium, Bandung, Indonesia), NaOH (AGC Chemicals, Thailand), and $AgNO_3$ (ROFA Laboratorium, Bandung, Indonesia). NaMMT is montmorillonite that has been calcined, acid-treated, and ion-exchanged with Na^+. 99% N_2 and CO_2 used for adsorption capacity tests was supplied by Sangkuriang Gas, Bandung, Indonesia.

Na-montmorillonite pillarization process mostly follows methods established by previous research (Hristodor et al. 2013). NaMMT was pillared using iron (III) hydroxide solution, which was previously prepared by mixing $FeCl_3$ with NaOH (mole ratio 1:2), then aging the solution for at least 24 h. Three solutions was prepared, each containing 0.025 M, 0.05 M, and 0.075 M of $FeCl_3$. The pillarization is done by stirring NaMMT in each solution for 24 h (50 mL solution per 1 g of NaMMT). Before pillarization, NaMMT was first swelled by mixing it with deionized water (12.5 mL per 1 g NaMMT) and stirring it for 15 min. The pillarized NaMMTs was then washed with deionized water to remove Cl^- ions (negative test done using 0.0282 N $AgNO_3$ solution), dried in an oven (110 °C) for 12 h, and calcined in air at 400 °C for 4 h. The calcination process causes the -OH bonds in $Fe(OH)_3$ to decompose, thus creating Fe_2O_3. The samples obtained were labelled as NaMMT-0.025, NaMMT-0.05, and NaMMT-0.075, respectively.

The carbon dioxide adsorption capacity of the samples was tested using thermogravimetric methods established by previous research (Chen & Lu 2015). In the first step, a small amount (roughly 5 mg) of sample was loaded to the thermogravimetric apparatus (Hitachi STA7300, PPNN ITB), then the samples were heated to 150 °C for 40 min in N_2 99% atmosphere (flow rate 100 mL/min). This is done to evaporate water and other impurities present. Then, the atmosphere was changed to CO_2 99% (flow rate 100 mL/min) and the temperature was cooled down to 30 °C (ramp rate 10 °C/min). This stage, including the time needed to cool the samples, lasted for 72 min. Finally, the atmosphere was changed back to N_2, and the temperature was heated again to 150 °C for another 40 min to desorb CO_2. Total time needed to complete the process is 176 min, with CO_2 adsorption occurring between the 52nd and 124th min. The mass of the samples was continuously measured during these steps, and then plotted with respect to time. CO_2 adsorption capacity (c_{CO2}) was determined by the difference between the weight of the sample after CO_2 adsorption (measured at the 124 th minute, m_b), and its weight before CO_2 adsorption (measured at the 52 nd minute, m_a). The weight difference was then divided by m_a before CO_2 adsorption. The resultant value was divided by m_a molar mass of CO_2 (44 gr/mol) to obtain the adsorption capacity value.

XRD patterns were taken at ambient conditions using Bruker D8 Advance (PPNN ITB) diffractometer, using Cu K α radiation ($\lambda = 1.54050$ Å; 40 kV and 40 mA) in the range $2\theta = 5 - 80°$. From the obtained diffractogram, Bragg's law was used to determine the interlayer spacing of the samples. FTIR spectra was obtained at ambient conditions using Shimatzu IRPrestige21 (Inorganic Chemistry Lab, Chemistry Department, ITB) with a DLATGS detector in the 4000-400 cm^{-1} region at 2 cm^{-1} resolution. XRF measurement was done using Bruker ORBIS EDAX (PPNN ITB) apparatus. BET-BJH analysis was done using N_2 adsorption-desorption in 77 K, using Nova 800 Anton Paar (Quantachrome) (Integrated Laboratory, UIN Sunan Kalijaga Yogyakarta).

RESULTS AND DISCUSSION

Thermogravimetric measurement results in the change of temperature and mass with respect to time for all samples. The resultant plot is given in Figure 1.

Some insights could be obtained from the data plotted in Figure 1. All samples show mass loss during the initial desorption process, and the time needed is relatively similar. After simultaneous switching of atmosphere to CO_2 and lowering of temperature, all samples are shown to had successfully adsorb CO_2. The shape of the graph shows that the adsorption process happens physically (Chen & Lu 2015). After the atmosphere was switched back to N_2, the mass for all samples reverted to the previous state, indicating CO_2 desorption. There is little difference between the mass of the samples before and after CO_2 desorption, indicating that nearly all CO_2 is desorbed.

Table 1 provides the CO_2 adsorption capacities for all samples. The data shows an increase in adsorption capacity for NaMMT-0.025 compared to NaMMT, whereas NaMMT-0.05 exhibited a decrease. On the other hand, NaMMT-0.075 demonstrated an increase in adsorption capacity compared to NaMMT, although the value was not as high as NaMMT-0.025. This result shows that there is an optimal amount of pillarizing species present in order to obtain maximum adsorption capacity, an observation also made by previous research (Wu et al. 2020). Table 2 presents the composition of the samples obtained through XRF analysis. The results clearly show an increase in Fe_2O_3 amount attributed to pillarization. The quantity of Fe_2O_3 directly increases with the increasing concentration of $FeCl_3$ used.
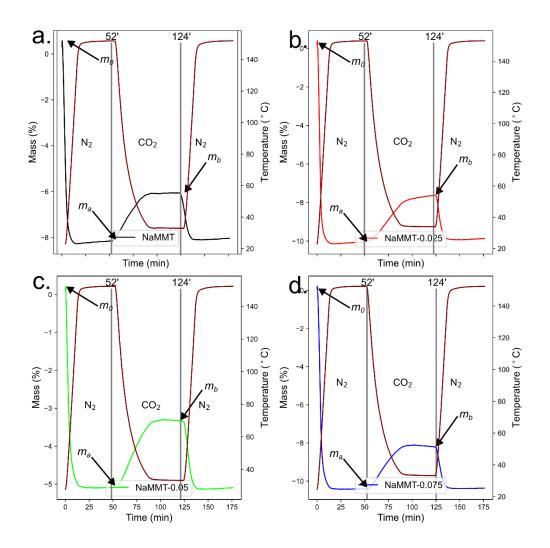
FIGURE 1. Mass and temperature change plot with respect to time for (a.) NaMMT, (b.) NaMMT-0.025, (c.) NaMMT-0.05, and (d.) NaMMT-0.075. The grey lines indicate the 52nd and 124th min position

TABLE 1. CO_2 adsorption capacity for all samples

Sample	m_0 (mg)	m_a (mg)	m_b (mg)	c_{CO2} (mmol/g)
NaMMT	5.026	4.616	4.722	0.518
NaMMT-0.025	4.841	4.355	4.472	0.608
NaMMT-0.05	4.960	4.707	4.794	0.417
NaMMT-0.075	4.993	4.421	4.529	0.556

TABLE 2. XRF measurement of the samples

Sample	Na_2O (wt.%)	Al_2O_3 (wt.%)	SiO_2 (wt.%)	K_2O (wt.%)	TiO_2 (wt.%)	V_2O_5 (wt.%)	Fe_2O_3
NaMMT	3.09	14.49	78.57	1.61	0.43	0.04	**1.78**
NaMMT-0.025	1.36	14.67	78.86	1.39	0.40	0.04	**3.27**
NaMMT-0.05	0.75	13.68	78.43	1.38	0.62	0.05	**5.10**
NaMMT-0.075	2.04	13.66	75.34	1.43	0.4	0.02	**7.11**

The XRD pattern of NaMMT and Fe_2O_3 pillarized NaMMT (NaMMT-0.025, NaMMT-0.05, NaMMT-0.075) is given in Figure 2(a). To aid visualization, the diffractogram of NaMMT-0.025, NaMMT-0.05, and NaMMT-0.075 is shifted vertically by 300, 600, and 900 units respectively. To identify the peaks, the pattern obtained was then compared to ICDD/JCPDS data (Gates-Rector & Blanton 2019).It was found that the samples contained montmorillonite (JCPDS 13-0135), quartz (JCPDS 46-1045), and muscovite (JCPDS 007-0042). Montmorillonite phases was identified at 8.88°, 17.81°, 19.80°, 27.89°, 34.80°and 61,80° , which belongs to [001], [003], [100], [005], [110], and [300] planes. Using Bragg's law, the crystal layer spacing (d_{hkl}) of each plane could be computed. It was found that each plane has a spacing of 9.94 (d_{001}), 4.74 (d_{003}), 4.47 (d_{100}), 2.58 (d_{005}), and 1.49 (d_{300}) Å respectively. The d_{001} peak position at 8.88° (2θ) was indicative of treated montmorillonites (Poppe et al. 2001). Pillarization caused decrease in intensity, peak broadening, and peak shifting, yet no major new peaks are identified. These changes are caused by pillar formation, which causes the material to be more amorphous in nature (Chauhan et al. 2022; Cottet et al. 2014; Li et al. 2022).

Special attention is paid to the peak located 20 = 8.88º (Figure 2 (b)), corresponding to plane. As more Fe_2O_3 is pillarized, the peaks become broader and the intensity lesser. However, little changes are observed in This is due to the nature of NaMMT as previously calcined montmorillonite, which loses its ability to expand and contract (Poppe et al. 2001).

Despite little changes observed in d_{001}, CO_2 adsorption capacity of the materials still differs significantly. This means that CO_2 adsorption changes could be attributed to the nature of Fe_2O_3 structures present on the material. When montmorillonites are pillared using metal oxides, significant differences happen based on the concentration of pillarizing material present (Salerno & Mendioroz 2002). In lower concentrations, the pillarization is incomplete, thereby disturbing the pore structures. At some concentration, all metal oxides are pillarized in the interlayer space of montmorillonite. Beyond this, the rest of the pillarizing agent instead forms an tetrahedrally-coordinated layer on the surface of montmorillonite. This formation does not contribute to the pillarization process. However, it still changes the overall textural properties, such as surface area and porosity, of montmorillonite.

The formation of this layer could be identified by FTIR. Because more Fe_2O_3 molecules are present in the surface of montmorillonite when it was arranged in a layer instead of pillarized, stronger interaction between Fe and Si-Al groups present in montmorillonite should be expected. FTIR spectra of NaMMT and Fe_2O_3 pillarized NaMMT (NaMMT-0.025, NaMMT-0.05, NaMMT-0.075) is given in Figure 3. To aid visualization, the spectra of NaMMT-0.025, NaMMT-0.05, and NaMMT-0.075 is shifted vertically by 100, 200, and 300 units, respectively. The resultant peaks were then identified by comparing it to literature.

The peaks located at 469, 525, 692, and 798 cm^{-1} corresponds to Si-O bending (Madejová 2003), Si-O-Al deformation (Madejová 2003), Si-O-Si stretching in quartz (Patel et al. 2006), and Fe-O-Si stretching, respectively (Sobhanardakani et al. 2018). The most notable peak is located at 1049 cm^{-1}, which corresponds to O-Si-O stretching in the tetrahedral layer of montmorillonite (Banik et al. 2015). The peak at 1630 cm^{-1} corresponds to H_2O molecule bending and stretching (Dongmo et al. 2020). Finally, peaks located at 3624 and 3448 cm^{-1} corresponds to Al-OH stretching and O-H symmetrical stretching (Dongmo et al. 2020; Tomul 2012), obtained from the water molecules present in the interlayer space.
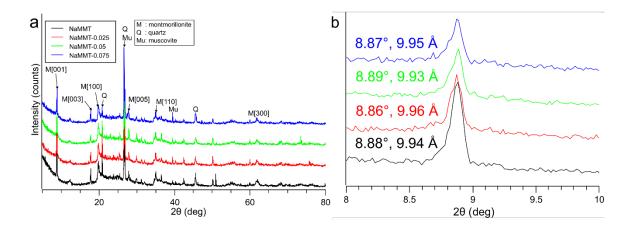
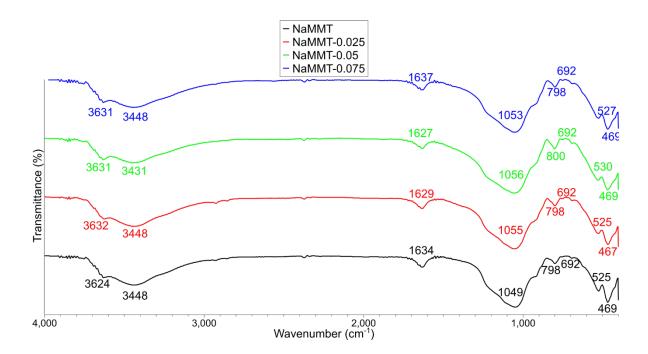FIGURE 2. (a) XRD pattern for all samples. (b) The [001] peak and d001, located at 2θ = 8.88°

FIGURE 3. FTIR spectra for all samples

Generally, few spectral differences compared to NaMMT were obtained from the spectra of pillared NaMMT. This shows that the structural form of montmorillonite does not change from pillarization and no chemical bonds was formed due to pillarization (Tomul 2012). Someshifts are observed, especially at aluminosilicate peaks located at 469, 525, 798, and 1049 cm -1 in NaMMT.

By comparing FTIR spectra of all samples, an interesting phenomenon is noted. Generally, more shifts are observed in NaMMT-0.05 compared to NaMMT-0.075, even though more Fe_2O_3 is present in NaMMT-0.075. This could be seen by comparing the changes in peak position and intensity of the aluminosilicate group peaks (469, 525, 798, and 1049 cm^{-1}), which was given in Tables 3 and 4.

TABLE 3. Aluminosilicate group peak position shift

Peak identification	NaMMT peak position (cm^{-1})	NaMMT-0.025 peak position (cm^{-1})	NaMMT-0.05 peak position (cm^{-1})	NaMMT-0.075 peak position (cm^{-1})
Si-O-Si bending	469	467	469	469
Si-O-Al stretching	525	525	530	527
Fe-O-Si stretching	798	798	800	798
Si-O-Si vibration	1049	1055	1056	1053

TABLE 4. Aluminosilicate group peak intensity shift

Peak identification	NaMMT peak intensity (%)	NaMMT-0.025 peak intensity (%)	NaMMT-0.05 peak intensity (%)	NaMMT-0.075 peak intensity (%)
Si-O-Si bending	20.90	19.50	12.31	15.56
Si-O-Al stretching	39.95	37.48	28.64	34.12
Fe-O-Si stretching	86.83	85.07	82.14	87.32
Si-O-Si vibration	12.52	11.86	6.89	10.38

Because formation of tetrahedral layers made more Fe_2O_3 interacts with aluminosilicate groups which shows up as stronger shifts in FTIR spectra, this suggests that more iron oxide by proportion is pillarized in NaMMT-0.075. To confirm this hypothesis, pore structure distribution (PSDs) of the samples must be obtained. Pillarization changes the porosity of the material by making smaller pillars. Moreover, it is also possible that less pores are formed due to thicker pillars. PSDs is obtained by analysing the N_2 adsorption-desorption isotherm of the samples, given in Figure 4.

The obtained isotherm plot is classified as IVa type plot with H3 type hysteresis based on IUPAC classification, which is typical for adsorption in mesoporous-microporous materials (Thommes et al. 2015). Pillarization causes less N_2 to be adsorbed, however, the amount of N_2 adsorbed did not change significantly with increasing amount of Fe_2O_3 present. This phenomenon happens due to more space being occupied by pillars (Salerno & Mendioroz 2002; Wu et al. 2020).

From the curve, BET-BJH analysis are performed to obtain the specific surface area (SSA), pore volume, and average pore diameter of the samples, which is shown and compared with the adsorption capacity of the material in Table 5.
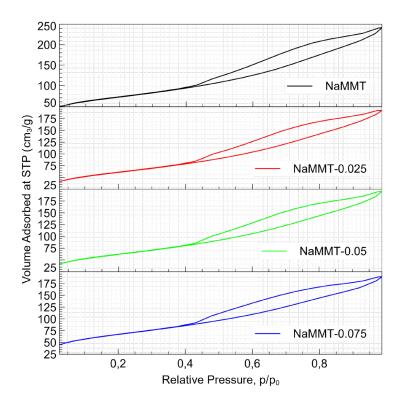
FIGURE 4. N$_2$ adsorption-desorption for all samples

TABLE 5. Pore parameters and CO$_2$ adsorption capacity of the samples

Sample	BET specific surface area (m^2/g)	Pore volume (BJH) (cm^3/g)	Average pore size (BJH) (nm)	Adsorption capacity (mmol/g)
NaMMT	254.95	0.374	5.865	0.518
NaMMT-0.025	215.56	0.299	5.539	0.608
NaMMT-0.05	219.40	0.303	5.521	0.417
NaMMT-0.075	236.70	0.293	4.957	0.556

The results indicate successful pillarization of Fe$_2$O$_3$, as indicated by decrease in specific surface area. It also shown that changes in specific surface area, pore volume, and average pore size are not completely consistent with CO$_2$ adsorption capacity of the samples, which indicates that the three measurements are not the only important factor affecting adsorption. This was also observed by previous research (Wu et al. 2020).

BJH model was then used to obtain the PSD, which is given in Figure 5. Pore distribution strongly influences the adsorption capacity of the material, and material with smaller pores and consistent size will have greater adsorption capacity (Lee & Park 2013).

Figure 5 shows that compared to NaMMT, NaMMT-0.025 shows reduced peak intensity and shift to lower pore diameter values. This shows that

pillarization is successfully performed, which causes more microporous (<2 nm) and less mesoporous (2-50 nm) pores to be formed. NaMMT-0.05 shows a roughly similar profile with NaMMT-0.025. However, the biggest pores in NaMMT-0.05 (115 nm) is much larger compared to other samples (99-100 nm). Finally, NaMMT-0.075 exhibit even more peak intensity reduction and shift to lower pore diameter values. This shows that even smaller pores are formed, and the number is less than other samples.

Appearance of bigger pores in NaMMT-0.05 suggests that less Fe_2O_3 is involved in pillar formation than other samples. This is consistent with the formation of tetrahedrally-coordinated iron atoms in the surface of NaMMT (Salerno & Mendioroz 2002). Bigger pores means montmorillonite are less able to

adsorb CO_2, due to weaker interactions (Busch et al. 2016). Conversely, smaller pores that was identified in NaMMT-0.075 suggests that the additional Fe_2O_3 (compared to NaMMT-0.05) is once again involved in pillar formation. Smaller pores mean more interaction between montmorillonite and CO_2, thus enabling NaMMT-0.075 to adsorb more CO_2 compared to NaMMT. However, the amount is less than NaMMT-0.025. This is most likely due to additional Fe_2O_3 causing less pores to appear, compared to NaMMT-0.025. Finally, it should be noted that the findings in NaMMT-0.075 is contrary to the conclusion made from previous research (Salerno & Mendioroz 2002), which states that after a certain concentration, only tetrahedrally-coordinated layers of pillaring atoms/molecules are formed in the interlayer space of montmorillonite.
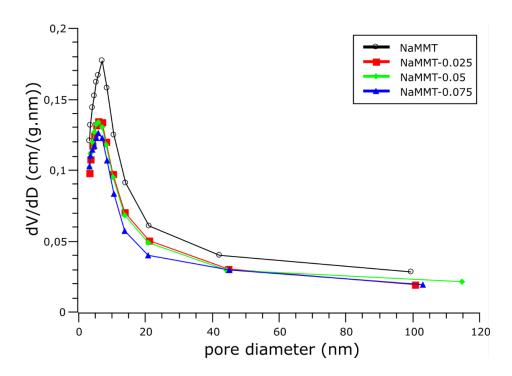

FIGURE 5. BJH pore size distribution for all samples

CONCLUSIONS

In conclusion, pillarization with Fe_2O_3 in appropriate amounts enable more carbon dioxide to be adsorbed compared to raw Na-montmorillonite. This is mainly due to the formation of less mesopores and more

micropores, enabling stronger interactions between CO_2 and montmorillonite. By varying the amount of Fe_2O_3 present, it was found that NaMMT-0.025 had the biggest amount of CO_2 adsorbed.

418

REFERENCES

Banik, N., Jahan, S., Mostofa, S., Kabir, H., Sharmin, N. Rahman, M. & Ahmed, S. 2015. Synthesis and characterization of organoclay modified with cetylpyridinium chloride. *Bangladesh J. Sci. Ind. Res.* 50: 65-70.

Bineesh, K.V., Kim, D-K., Cho, H-J. & Park, D-W. 2010. Synthesis of metal-oxide pillared montmorillonite clay for the selective catalytic oxidation of H_2S. *Journal of Industrial and Engineering Chemistry* 16(4): 593-597.

Bouazizi, N., Barrimo, D., Nousir, S., Ben Slama, R., Roy, R. & Azzouz, A. 2017. Montmorillonite-supported Pd^0, Fe^0, Cu^0 and Ag^0 nanoparticles: Properties and affinity towards CO_2. *Applied Surface Science* 402: 314-322.

Busch, A., Bertier, P., Gensterblum, Y., Rother, G., Spiers, C.J., Zhang, M. & Wentinck, H.M. 2016. On sorption and swelling of CO_2 in clays. *Geomech. Geophys. Geo-Energ. Geo-Resour.* 2: 111-130.

Chauhan, T., Udayakumar, M., Ahmed Shehab, M., Kristály, F., Katalin Leskó, A., Ek, M., Wahlqvist, D., Tóth, P., Hernadi, K. & Németh, Z. 2022. Synthesis, characterization, and challenges faced during the preparation of zirconium pillared clays. *Arabian Journal of Chemistry* 15: 103706.

Chen, Y-H. & Lu, D-L. 2015. CO_2 capture by kaolinite and its adsorption mechanicm. *Applied Clay Science* 104: 221-228.

Cottet, L., Almeida, C.A.P., Naidek, N., Viante, M.F., Lopes, M.C. & Debacher, N.A. 2014. Adsorption characteristics of montmorillonite clay modified with iron oxide with respect to methylene blue in aqueous media. *Applied Clay Science* 95: 25-31.

Desai, H., Kannan, A. & Reddy, G.S.K. 2023. Sustainable and rapid pillared clay synthesis with applications in removal of anionic and cationic dyes. *Microporous and Mesoporous Materials* 352: 112488.

Dongmo, L.M., Jiokeng, S.L.Z., Pecheu, C.N., Walcarius, A. & Tonle, I.K. 2020. Amino-grafting of montmorillonite improved by acid activation and application to the electroanalysis of catechol. *Applied Clay Science* 191: 105602.

Eggleton, T. 2012. *A Short Introduction to Climate Change*. Cambridge: Cambridge University Press.

Feng, B., Wei, Y., Qiu, Y., Zuo, S. & Ye, N. 2018. Ce-modified AlZr pillared clays supported-transition metals for catalytic combustion of chlorobenzene. *Journal of Rare Earths* 36: 1169-1174.

Gates-Rector, S. & Blanton, T. 2019. The powder diffraction file: A quality materials characterization database. *Powder Diffr.* 34(4): 352-360.

Hristodor, C-M., Vrinceanu, N., Pode, R., Copcia, V.E., Botezatu, E. & Popovici, E. 2013. Preparation and thermal stability of Al_2O_3-clay and Fe_2O_3-clay nanocomposites, with potential application as remediation of radioactive effluents. *J. Therm. Anal. Calorim.* 111: 1227-1234.

Kumararaja, P., Manjaiah, K.M., Datta, S.C. & Sarkar, B. 2017. Remediation of metal contaminated soil by aluminium pillared bentonite: Synthesis, characterisation, equilibrium study and plant growth experiment. *Applied Clay Science* 137: 115-122.

Lee, S-Y. & Park, S-J. 2013. Determination of the optimal pore size for improved CO_2 adsorption in activated carbon fibers. *Journal of Colloid and Interface Science* 389(1): 230-235.

Li, Q., Sun, X., Zhang, W., Sun, Z., Na, S., Chen, Z., Wang, L., Yuan, C. & Sun, H. 2022. Effect of Fe(III)-modified montmorillonite on arsenic oxidation and anthracene transformation in soil. *Science of The Total Environment* 814: 151939.

Madejová, J. 2003. FTIR techniques in clay mineral studies. *Vibrational Spectroscopy* 31: 1-10.

Marco-Brown, J.L., Barbosa-Lema, C.M., Torres Sánchez, R.M., Mercader, R.C. & Dos Santos Afonso, M. 2012. Adsorption of picloram herbicide on iron oxide pillared montmorillonite. *Applied Clay Science* 58: 25-33.

Patel, H.A., Somani, R.S., Bajaj, H.C. & Jasra, R.V. 2006. Nanoclays for polymer nanocomposites, paints, inks, greases and cosmetics formulations, drug delivery vehicle and waste water treatment. *Bull. Mater. Sci.* 29: 133-145.

Poppe, L.J., Paskevich, V.F., Hathaway, J.C. & Blackwood, D.S. 2001. *A Laboratory Manual for X-Ray Powder Diffraction*. https://doi.org/10.3133/ofr0141

Quiroz-Estrada, K., Hernández-Espinosa, M.A., Rojas, F., Portillo, R., Rubio, E., López, L. 2016. N_2 and CO_2 adsorption by soils with high kaolinite content from San Juan Amecac, Puebla, México. *Minerals* 6(3): 73.

Raganati, F., Miccio, F. & Ammendola, P. 2021. Adsorption of carbon dioxide for post-combustion capture: A review. *Energy Fuels* 35(16): 12845-12868.

Rubin, E., Abanades, J.C., Akai, M., Benson, S., Keith, D., Mazzotti, M., Metz, B., Osman-Elasha, B., Palmer, A., Smekens, K. & Soltanieh, M. 2005. *IPCC Special Report : Carbon Dioxide Capture and Storage*, 1st ed. Cambridge: Cambridge University Press.

Ruiz-Torres, C.A., Araujo-Martínez, R.F., Martínez-Castañón, G.A., Morales-Sánchez, J.E., Guajardo-Pacheco, J.M., González-Hernández, J., Lee, T-J., Shin, H-S., Hwang, Y. & Ruiz, F. 2018. Preparation of air stable nanoscale zero valent iron functionalized by ethylene glycol without inert condition. *Chemical Engineering Journal* 336: 112-122.

Salerno, P. & Mendioroz, S. 2002. Preparation of A1-pillared montmorillonite from concentrated dispersions. *Applied Clay Science* 22(3): 115-123.

Sobhanardakani, S., Jafari, A., Zandipak, R. & Meidanchi, A. 2018. Removal of heavy metal (Hg(II) and Cr(VI)) ions from aqueous solutions using $Fe_2O_3@SiO_2$ thin films as a novel adsorbent *Process Safety and Environmental Protection* 120: 348-357.

Thommes, M., Kaneko, K., Neimark, A.V., Olivier, J.P., Rodriguez-Reinoso, F., Rouquerol, J. & Sing, K.S.W. 2015. Physisorption of gases, with special reference to the evaluation of surface area and pore size distribution (IUPAC Technical Report). *Pure and Applied Chemistry* 87(9-10): 1051-1069.

Tomul, F. 2012. Influence of synthesis conditions on the physicochemical properties and catalytic activity of Fe/Cr-pillared bentonites. *Journal of Nanomaterials* 2012: 237853.

Wang, X., Cheng, H., Chai, P., Bian, J., Wang, X., Liu, Y., Yin, X., Pan, S. & Pan, Z. 2020. Pore characterization of different clay minerals and its impact on methane adsorption capacity. *Energy Fuels* 34(10): 12204-12214.

Wu, K., Ye, Q., Wu, R., Chen, S. & Dai, H. 2020. Carbon dioxide adsorption behaviours of aluminum-pillared montmorillonite-supported alkaline earth metals. *Journal of Environmental Sciences* 98: 109-117.

*Corresponding author; email: triati@itb.ac.id